Tuijin Jishu/Journal of Propulsion Technology
ISSN: 1001-4055
Vol. 45 No. 4 (2024)

Early Tuberculosis Detection using Advanced Feature Extraction Techniques Integrated with a PSO-GWO-Based Neural Network Classifier

Gitesh S. Gujrathi [1] , Dr. Mukesh Yadav [2]

1 Ph.D. Scholar, SAGE University, Indore, India

2 Ph.D.Guide, HOD, Electronics & Telecommunication Department, SAGE University, Indore, India

Abstract:

The global health challenge posed by Tuberculosis (TB) necessitates innovative solutions for early detection, especially in regions heavily burdened by the disease. This paper introduces a groundbreaking approach—an automated computer-aided diagnosis system aimed at reducing reliance on expert radiologists for early TB detection through chest X-ray images. The proposed technique leverages advanced feature extraction methods, including GLCM, HOG, and DWT-GIST Descriptor coefficients, and employs a PSO-GWO based Neural Network (NN) classifier. This integration of sophisticated techniques contributes to a comprehensive and accurate TB detection system. The evaluation results demonstrate an impressive accuracy of 97.12%, highlighting the potential of the proposed approach to significantly improve the efficiency and accessibility of TB diagnosis, particularly in resource-constrained settings where expert radiologists may be scarce. This innovative system represents a crucial step towards addressing the challenges associated with TB diagnosis, offering a promising solution for timely and accurate detection.

Keywords –Chest X-Ray, Discrete Wavelet Transform, Gray-Level Co-occurrence Matrix, Grey Wolf Optimization, Histogram of Oriented Gradients, Neural Network, Particle Swarm Optimization, Tuberculosis.

1. INTRODUCTION

Timely identification plays a pivotal role in effectively combating tuberculosis (TB), as early detection can significantly reduce mortality rates. Unfortunately, in regions with inadequate medical facilities, particularly in underdeveloped countries, early detection efforts face considerable challenges. Despite the effectiveness of antibiotics in treating TB, the disease still exhibits a high mortality rate, indicating that cases either go unnoticed or are identified in advanced stages.

Common techniques for TB detection encompass Sputum Smear Microscopy and chest X-ray (CXR), with the latter proving more sensitive than verbal screening in identifying pulmonary TB. However, while CXR is effective, it presents challenges, particularly the necessity for skilled personnel to interpret CXR images. TB manifests in various lung patterns, including infiltrates, consolidation, and cavitation. This paper underscores the significance of addressing these challenges in TB detection, emphasizing the requirement for accessible and dependable diagnostic methods to effectively combat this global health threat. The inclusion of sample CXR images illustrating diverse TB manifestations serves to elucidate the intricacies of the diagnosis process.

A standard Computer-Aided Diagnosis (CAD) system for TB detection consists of three vital stages: lung field segmentation, feature extraction, and classification. In the context of chest X-rays (CXRs), lung segmentation is frequently utilized as a pre-processing step to extract the region of interest (ROI), crucial for subsequent analysis. Notably, precise clavicle segmentation abnormalities can play a crucial role in early diagnosis, particularly as TB and numerous lung diseases commonly manifest in the lung apex. Segmentation also facilitates region-based processing, encompassing contrast enhancement and bone suppression.

Following segmentation, the subsequent step involves extracting visual features effectively representing these ROIs. Various texture features (e.g., wavelets, local binary pattern) and shape features (e.g., ellipticity, circularity), either independently or in combination, are utilized to characterize lung regions. Additionally, a variety of classifiers, including Support Vector Machine (SVM), Neural Network (NN), Random Forest (RF), and Bayesian Network (BN), are investigated for CXR classification as normal or abnormal.

The emergence of deep learning (DL) algorithms, particularly deep convolutional neural networks (DCNN), has marked significant strides in developing systems for pulmonary TB detection. DCNN, a form of supervised machine learning algorithm, incorporates multiple convolution layers, pooling layers, and fully-connected layers. Notably, DCNN, especially in the guise of Convolutional Neural Network (CNN) models, displays promise due to its capacity to learn parameters and extract global and local features from extensive datasets. In contrast to handcrafted features, CNN models do not necessitate domain-specific knowledge and offer robust feature representation capabilities.

2. LITERATURE REVIEW

The exploration of tuberculosis diagnosis has been extensively addressed in scholarly works, with diverse methodologies striving to achieve optimal accuracy in diagnostic systems. Our investigation distinguishes itself by delving into deep learning models, extracting features, and seamlessly integrating them with attributes derived from texture, shape, and geometry through GLCM, DWT, and LBP algorithms. Our classification process employs hybrid techniques, prioritizing both accuracy and effectiveness in the realm of tuberculosis diagnosis. In the subsequent discussion, we delve into various research endeavors related to tuberculosis diagnosis, focusing on those leveraging deep learning.

For instance, the authors of introduced a model rooted in Deep Convolutional Neural Networks (DCNN) for diagnosing chest X-rays, conducting evaluations on a distinct dataset. Their findings underscore a common challenge encountered in deep learning models, where performance achieved on a specific training dataset may not translate equally well when applied to a disparate dataset. While effective within its designed context, the technology's applicability to diverse datasets is constrained. In another study, the authors of proposed an automated recognition system for signs of cavities in lung computed tomography (CT). They integrated handcrafted and deep features, employing hybrid resampling techniques, and found that combining multiple features surpassed individual feature classes, attaining commendable sensitivity. Another study, presented a multi-level similarity technique for identifying common signs of lung diseases in lung CT scans.Moving forward, the authors of suggested an SVM algorithm for discriminating pulmonary tuberculosis from other lung diseases. The algorithm leans on discriminatory features for image classification. While the algorithm's performance highlights the significance of bronchiectasis in identifying crucial characteristics, achieving an accuracy of 85% and a sensitivity of 88%, its drawback lies in not attaining satisfactory accuracy despite extracting representative features. In a different vein, the authors of refined SVM algorithms for classifying chest X-rays based on texture features extracted using the Wavelet Transform (WT) method. A genetic algorithm was employed for feature selection, showcasing the method's advantage, yet it suffers from the drawback that the selected features are not tested on more than one classifier.

Another noteworthy development comes from the authors of who crafted an EfficientNets model for tuberculosis diagnosis using two detection datasets. Employing five types of EfficientNets, with efficientNet-b4 yielding the best performance at an accuracy of 92.33%, this approach's strength lies in applying multiple EfficientNets for tuberculosis diagnosis. However, the limitation is evident in its failure to achieve consistently high accuracy. Furthermore, the authors of introduced a deep convolutional network based on the generative adversarial network, incorporating three distinct structures for optimizing, generating, segmenting, and classifying chest X-ray images. This comprehensive approach strives to enhance various facets of image analysis for diagnostic purposes.

In conclusion, these investigations deploy diverse methodologies, including SVM algorithms, improved SVMs with genetic algorithms, EfficientNets, and deep convolutional networks, for tuberculosis diagnosis using chest X-ray images. While each approach boasts unique advantages, such as feature extraction and selection

algorithms, and the integration of multiple networks, they simultaneously encounter challenges, particularly in achieving consistently high accuracy. These insights contribute to the ongoing endeavors to refine and optimize tuberculosis diagnostic methodologies.

3. MATERIALS AND METHODS

A. Histogram of Oriented Gradients (HOG)

The HOG algorithm calculates the distribution of gradient orientations within localized image regions. Primarily employed for object detection, it also effectively captures texture information. This method entails computing histograms of gradient directions within specific regions of the input image. Areas surrounding edges and corners typically yield higher gradient values, furnishing more detailed object shape information compared to flat regions. The 80×80 image matrix undergoes computation of gradient magnitude and direction for each pixel, followed by segmentation into multiple 16×16 blocks. Each block comprises four cells, each covering an 8×8 pixel area.HOGsare individually computed for each cell, with distribution across nine histogram bins spanning angles from 0 to 180 degrees, each bin covering a 20-degree range. Pixel assignment to a particular bin is based on its direction and corresponding magnitude values. The four adjacent cells of size 8×8 amalgamate into a single 16×16 block, resulting in 36 HOG constants (9 bins × 4 cells). The ultimate HOG features for the entire image are derived through a 50% overlap for each block. In an 81-block LSB matrix with overlap, the aggregate number of HOG features totals 2916 (81 blocks × 36 constants).

B. GIST Descriptor

The primary goal of the GIST descriptor is to generate condensed data that contains adequate information for recognizing specific elements within images. This methodology emphasizes the components of a figure by establishing a correlation between the outline of a region and its attributes. Notably, it dismisses smaller objects in the image along with their significance. Human observations, including genuineness, directness, unevenness, extension, and roughness, are utilized as expressive remarks, portraying the spatial structure of the image.

The calculation process for the universal GIST descriptor involves the extraction of spatial, frequency, and orientation information. This is achieved by convolving the CXR image with 32 Gabor filters spanning four scales and eight directions, resulting in 32 feature maps of the same size as the original image. Subsequently, the image is partitioned into 4×4 grids, creating 16 regions, and the average feature values within each region are computed. This yields a total of 512 features, with 32 features assigned to each region across the 16 regions, encapsulating essential characteristics for a comprehensive representation of the image.

C. Artificial Neural Network Classifier

Constructed upon the neural networks inherent in human brains, this system comprises three distinct layers. The initial layer, consisting of a solitary layer, is tasked with processing the input data.It accepts the ultimate features as inputs, performs computations through its neurons, and subsequently transfers the data to the subsequent hidden layers. Positioned between the input and output layers are multiple hidden layers. The output layer gathers information from the hidden layer and disseminates it beyond the network. The quantity of nodes in the output layer aligns with the desired outputs.

D. Feature Extraction using GLCM

The GLCM emerges as a valuable technique in the realms of image processing and computer vision, offering insights into image texture. The creation of a GLCM involves a meticulous consideration of pixel pairs' relative positions within an image, tallying occurrences of specific gray level pairs at these positions. Essentially, a GLCM serves as a histogram, delineating the frequency of co-occurring gray levels in an image and revealing spatial relationships among pixel intensities. The versatility of GLCM manifests in its ability to be computed for distinct directions and distances, facilitating the extraction of diverse texture features like contrast, energy, homogeneity, and entropy. These extracted features find applications in image classification, object recognition, and texture analysis. Notably, GLCM proves instrumental in distinguishing between textures such as smooth, rough, or repetitive patterns, making it particularly valuable in medical image analysis.Texture, defined as the

recurrence of patterns across a region, exhibits various qualities, including fine, rough, smooth, random, or striped. The statistical nature of texture properties follows a quadratic pattern, comparing gray level differences between pixels at distinct locations. Different textures unveil themselves through the revelation of texture properties, ascertainable via various methods, including GLCM, first-order slope distributions, and edge co-occurrence matrices.In the present study, the focus lies on extracting texture features using GLCM, grounded in the estimation of the second-order composite state probability density function, $P(i,j|d,\theta)$. This matrix encapsulates the likelihood of transitioning from gray level i to gray level j at a specific distance (d) and angle (θ) between pixels. To ensure rotational invariance, a square matrix is employed, and investigations occur in four directions—usually $\theta = 0^{\circ}, 45^{\circ}, 90^{\circ}$, and 135° (refer to Figure 1). Haralick recommends averaging the features obtained from the GLCM computed in these directions. Generally, distance values of $d = 1, 2$ are preferred.

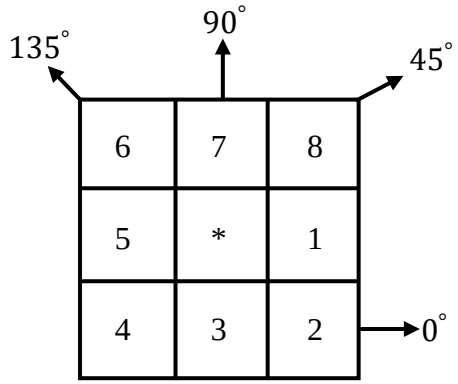

Figure 1: Gray Level Co-occurrence Matrix

For this work, GLCMs with $d = 1$ and $\theta = 0^{\circ}, 45^{\circ}, 90^{\circ}$, and 135° values were created by moving the 5×5 window over the images. From these matrices, five properties including energy, contrast, correlation, homogeneity and entropy, which include the texture characteristic of the image, are found.

$$Energy = \sum_{i,j} P_{ij}^2 \quad (1)$$

$$Contrast = \sum_{i,j} |i-j|^2 P_{ij} \quad (2)$$

$$Correlation = \frac{\sum_{i,j}(i,j)P_{ij} - \mu_x \mu_y}{\sigma_x \sigma_y} \quad (3)$$

$$Homogeneity = \sum_{i,j} \frac{P_{ij}}{1+|i-j|} \quad (4)$$

$$Entropy = -\sum_{i,j} P_{ij} \log P_{ij} \quad (5)$$

The values denoted as μ_x, μ_y, σ_x, and σ_y in this context represent the average and variability of the rows and columns within the probability density function P_{ij}.

The energy, contrast, correlation, homogeneity, and entropy features obtained from theGLCMare commonly used to describe the texture and structural properties of an image. These features provide information about the local intensity relationships between the pixels in the image and can be used to distinguish between different textures and structures in the image. The energy, contrast, and correlation features are often used to describe the texture of an image, while the homogeneity and entropy features are used to describe the spatial distribution of the gray levels in the image.

By computing these features from the GLCM, one can obtain a rich set of texture and structural descriptors that can be used for various image processing tasks, such as image segmentation, pattern recognition, and feature extraction. The GLCM-based features are particularly useful for character recognition because they can provide information about the texture and structure of the characters, which can be used to distinguish between different characters and improve the recognition accuracy.

4. PROPOSED METHODOLOGY

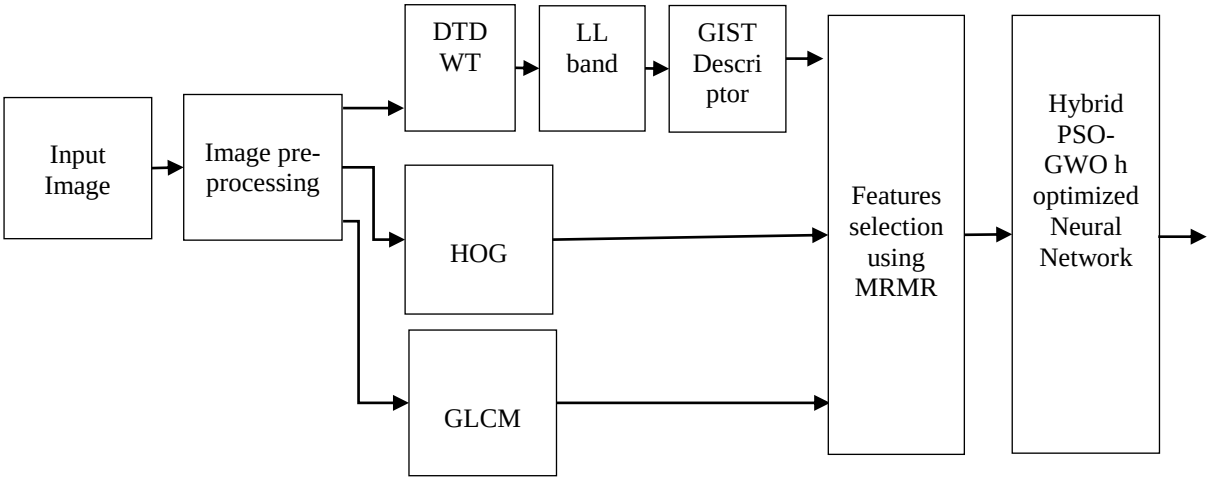

Figure 2: Proposed methods for tuberculosis diseases recognition

A. Compressed Hybrid Domain Tuberculosis Diseases Recognition Algorithm-1

The proposed Compressed Hybrid Domain Tuberculosis Diseases Recognition Algorithm 1, outlined in Table 1, focuses on Human Recognition using Compact Histogram, DWT, and Double Density Dual Tree Discrete Wavelet Transform (DDDTDWT) applied to CXR Images captured in Uncontrolled Conditions. The algorithm generates three sets of features: Histogram Intensities, DWT, and DDDTDWT.

The first set of features is obtained from the Histogram, considering only 200 out of 256 prominent intensities. The second set of features is derived using DWT, with only the approximating LL band coefficients considered, resulting in a reduced feature set size of $1/4^{th}$of the original (120×160=19200). The third set of features, with a dimension of 4800, is extracted at the fifth-level band coefficients using DDDTDWT.

By concatenating these three robust and compressed feature sets, each with sizes of 24200, the final feature set is obtained. Recognition accuracy is assessed using the Euclidean Distance (ED) metric, which measures the similarity between the features of the test CXR picture and those in the database.

Table 1: Compressed Hybrid Domain X-Ray Recognition Algorithm 1

Input: x-ray images from benchmarked databases.
Output: Accuracy of identification is computed.
1. Utilize regular databases of X-ray images to evaluate the proposed method.

2. Resize X-ray images of varying sizes from different databases to a uniform size of 240×320. Convert color photographs to grayscale versions.
3. Apply histogram analysis to a 240×320 X-ray image, resulting in 76800-dimensional histogram coefficients. Only 200 key values are considered in the first batch.
4. Analyze X-ray images using Discrete Wavelet Transform (DWT), focusing on the first level LL band with a size of 120×160 (19200) as the second set of initial features.
5. Apply DDDTDWT to X-ray images, considering the third set of initial features with a dimension of 4800.
6. Concatenate histogram coefficients, LL band coefficients, and DDDTDWT fifth band coefficients to obtain the final feature set of 24200.
7. Achieve a compression ratio of 68.49% for the final features.
8. Evaluate the proposed model by employing the Euclidean Distance (ED) formula between X-ray images in the database and test images.
9. Compute the model's accuracy to obtain the result R1.

B. Compressed Hybrid Domain Tuberculosis Detection Algorithm-2

Table 2 introduces an effective hybrid domain feature extraction approach for the identification of tuberculosis. This method integrates binary pixel segmentation, DWT, HOG, and the GIST descriptor. The binary pixels are subsequently divided into Most Significant Bits (MSB) and Least Significant Bits (LSB). Each 4-bit binary segment undergoes conversion into corresponding decimal values and is reshaped into an 80×80 matrix.

Both MSB and LSB matrices undergo the application of DWT and HOG. The GIST descriptor is specifically employed on the LL-sub band of DWT, extracting the initial set of features, while the second set comprises HOG features. The combination of GIST and HOG features, accomplished through convolution, yields the ultimate and compelling feature set. The classification of these features for CXR image databases and test images is executed via an ANN to assess the system's efficacy.

Table 2: Compressed Hybrid Domain X-Ray Recognition Algorithm 2

Input: Benchmarked x-ray image databases.

Output: Accuracy of identification is computed.

1. Employ the regular x-ray image databases for evaluating the proposed technique.
2. resizing the detected x-ray images to 80×80.
3. Convert each pixel's decimal value to binary and segment it into MSB and LSB.
4. Reconstruct images from MSB and LSB, resulting in a size of 80×80.
5. Apply DWT to the MSB image, considering the LL band coefficient matrix with a size of 40x40.
6. Employ the GIST Descriptor on the LL band matrix, generating 640 coefficients.
7. Apply HOG on the LSB image, yielding 2916 coefficients.
8. Convolve the 640 GIST Descriptor coefficients with the 2916 HOG coefficients to obtain the final set of 3555 features.
9. Employ an Artificial Neural Network Classifier to evaluate the proposed model.
10. Compute the model's accuracy to obtain result R2.

C. PSO-GWO-NN Classifier

This section provides a detailed description of the optimal design process, employing the PSO-GWO hybrid algorithm. The approach integrates the strengths of both PSO and GWO to efficiently explore the parameter space and determine the optimal neural network weight parameters.

1. Particle Swarm Optimization (PSO)

PSO represents an optimization algorithm grounded in the collective behavior observed in bird flocks or fish schools. Within the PSO framework, a population, termed particles, explores the search space to identify the optimal solution. Every particle adapts its position by drawing insights from its individual experiences and the collective experience of the most successful particle within the population.

The position update equation for each particle in PSO is given by:

$$X_i^{(t+1)} = X_i^{(t)} + V_i^{(t+1)}$$

(6)

Where:

- $X_i^{(t+1)}$ is the updated position of particle i in the t+1 iteration,
- $V_i^{(t+1)}$ is the velocity of particle i in the t+1 iteration.

The velocity is updated using both personal best (P_{best}) and global best (G_{best}) information.

2. Grey Wolf Optimization (GWO)

GWO is inspired by the hunting behavior of grey wolves and is a metaheuristic optimization algorithm. In GWO, three types of wolves (alpha, beta, and delta) are assumed to lead the pack. Wolves adjust their positions based on the positions of these leaders.

The position update equation for each wolf in GWO is given by:

$$X_i^{(t+1)} = X_\alpha^{(t)} - A \cdot D_i^{(t)}$$

(7)

Where:

- $X_i^{(t+1)}$ is the updated position of wolf i in the $t+1$iteration,
- $X_\alpha^{(t)}$ is the position of the alpha wolf in the $t$iteration,
- A is a coefficient,
- $D_i^{(t)}$ is a random vector.

3. PSO-GWO Hybrid Optimization

The hybrid optimization technique, combining the PSO and GWO algorithms, harnesses the unique strengths inherent in each. In every iteration, the PSO algorithm steers the population toward promising sectors within the search space. Subsequently, the GWO algorithm comes into play, strategically exploiting these identified regions for enhanced performance.

The comprehensive hybrid optimization unfolds through the following sequential steps:

- Initialization: Kickstart the particle population with randomly assigned positions and velocities.
- Fitness Evaluation: Gauge the fitness of each particle by applying the objective function, wherein, for neural network design, the MSE method is employed.
- PSO Update: Refine the position and velocity of each particle through the application of the PSO algorithm.
- GWO Exploitation: Transition to GWO after a predefined number of iterations or upon meeting specific criteria, intensifying the exploitation of promising regions pinpointed by PSO.
- Optimal Solution: Determine the optimal solution by assessing the best-performing outcome achieved throughout the entirety of the hybrid optimization process.

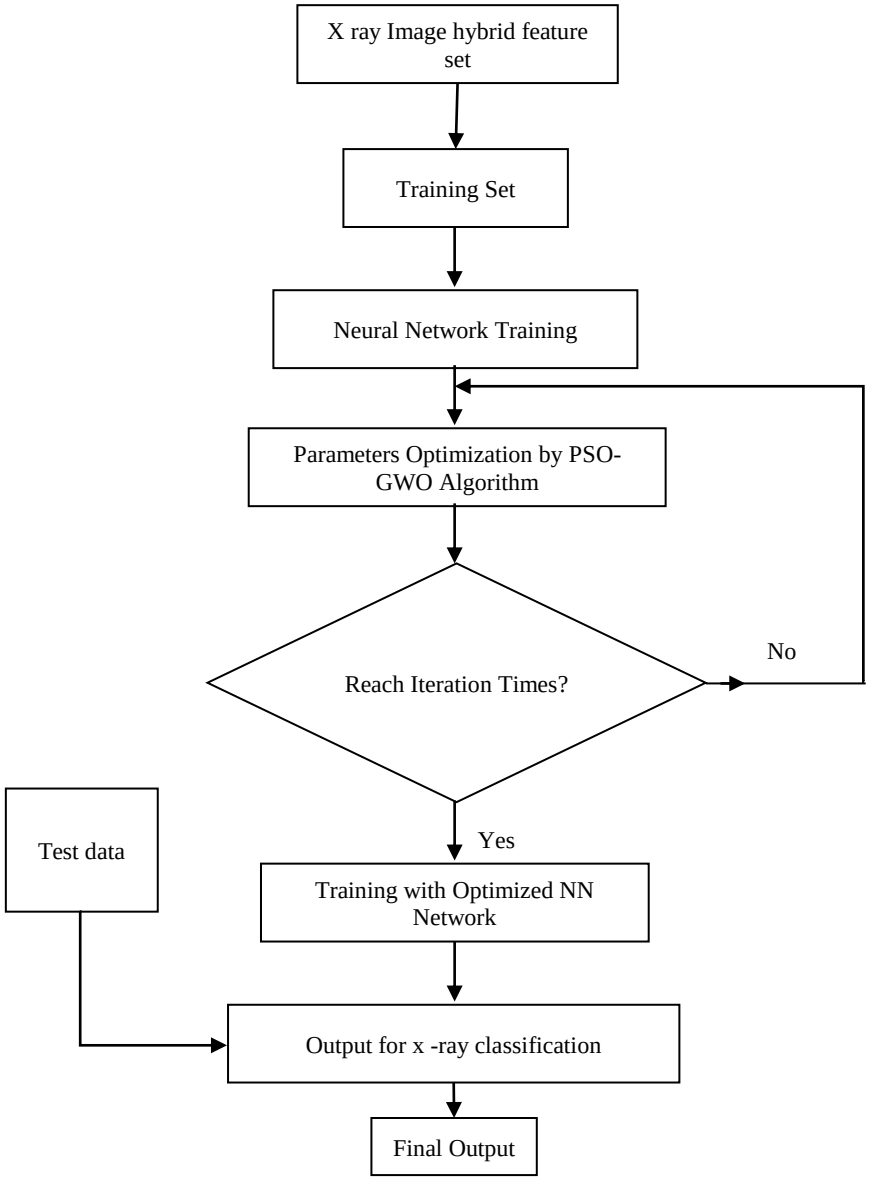

Figure 3: Schematic representation illustrating the optimized model derived from the PSO-GWO-Optimized Neural Network

D. Objective Function

The objective function in the context of training an artificial neural network (ANN) serves as a metric to be minimized, reflecting the error or loss in the learning process. In this paper, the chosen metric for evaluating the performance of the ANN during training is the Mean Square Error (MSE). The Mean Square Error quantifies the average squared difference between the predicted outputs generated by the neural network and the actual outputs corresponding to a given set of training patterns. By calculating the squared differences and averaging them, the MSE provides a comprehensive measure of the overall accuracy or precision of the network's predictions in relation to the desired outcomes. Minimizing the Mean Square Error is a common optimization goal during the training phase, aiming to enhance the network's ability to approximate the target outputs accurately.

$$\hat{w} = \min_{w \in \mathbb{R}^d} f(w, X)$$

(8)

$$f(w, X) = \frac{\sum_{i=1}^{|X|} (\hat{y}_l - y_i)^2}{|X|}$$

(9)

Where:

- w is the weight vector of the ANN.
- X is the set of training patterns.
- $\hat{y}_l$ is the expected output for pattern x_i.
- y_i is the actual output for pattern x_i.
- $|X|$ is the number of training patterns.

E. Training the Neural Network

The neural network undergoes training using the optimal weight vector obtained through the hybrid optimization process. The choice between using either w_best or w_best' is determined based on which of the two resulted in a lower Mean Square Error (MSE). The selection of the best weight vector is crucial as it directly influences the network's ability to minimize the prediction error during training. By employing the weight vector associated with the lower MSE, the neural network aims to enhance its learning and predictive capabilities, ultimately improving its performance on the given task. This adaptive approach ensures that the network utilizes the most effective set of weights for achieving optimal results based on the specific optimization process undertaken.

ANNs are computational models inspired by the functioning of the human brain, particularly the interconnected neurons. ANNs are powerful machine learning models used for various tasks, including image classification. In this explanation, we will formulate an ANN classifier for predicting Tuberculosis (TB) using Chest X-ray images with GLCM-based texture feature extraction.

- ***Input Data Representation:*** Let's denote our dataset of Chest X-ray images as X, where each image is represented as a matrix. For instance, a single Chest X-ray image of size (height H, width W, and number of channels C) will be represented as $X \in \mathbb{R}^{H \times W \times C}$.
- ***Feature Extraction using GLCM:*** As mentioned in the methodology, GLCM-based texture feature extraction is performed on each pre-processed Chest X-ray image. The GLCM calculates the co-occurrence of pixel values at a specific distance and angle within the image. The resulting texture features, such as contrast, energy, homogeneity, and correlation, are obtained for each image.Let F be the feature vector obtained from the GLCM-based texture feature extraction for a single image. Thus, $F = [f_1, f_2, \ldots, f_n]$, where n is the number of texture features extracted.

5. Simulation and Results

A. Dataset

This research work is based on two datasets published in the KAGGLE data science community by the authors of when combining the two data sets give a total of 7662 images of chest radiographs of anonymized patients, the objective of unifying the two datasets is to have greater variability in the data, when training the algorithms, they can generalize adequately before different image sources in the validation and test stage.

An analysis of each image is performed to discard those with noise; that is, they are not correspond to one of the classes, they are illegible, they will be superimposed black or white texts or boxes, poor positioning, among other aspects that made these images not meet the characteristics of each class of the dataset. After cleaning of invalid data that could generate noise when training the algorithms, a dataset of a total of 5,748 images remained, 2,905 images of healthy patients and 2,843 images of patients with tuberculosis. The dataset will be divided into two sets, the training set with 80% and the test set with 20% of the total. Out of the total training

data, it will be divided again into data for training and data for validation, in this case of the total training data, 20% will be used for cross-validation in the training stage. A sample can be seen in Figure 4.

(a) Normal (b) Tuberculosis

Figure 4: Images of a healthy patient and a patient with tuberculosis [11]

B. Evaluation Parameters

The confusion matrix, comprised of the initial quartet: True positive, false negative, false positive, and True negative. This matrix proved highly valuable, primarily for two reasons: firstly, as its data encapsulated the outcomes of Tuberculosis disease detection, and secondly, it served as the conduit for acquiring the remaining metrics.

Table 3: Evaluation parameters

TP (True Positive)	"Indicated the number of Tuberculosis disease that were classified as correctly classified"
TN (True Negative)	"Indicated the number of Tuberculosis disease that were classified as not classified correctly"
FP (False Positive)	"Indicated the number of Tuberculosis disease that were classified as incorrectly classified"
FN (False Negative)	"Indicated the number of Tuberculosis disease that were classified as not classified incorrectly"

$$Accuracy = \frac{TP+TN}{TP+TN+FP+FN} \quad (10)$$

$$Precision = \frac{TP}{TP+FP} \quad (11)$$

$$Sensitivity = \frac{TP}{TP+FN} \quad (12)$$

$$F-Score = \frac{2TP}{2TP+FP+FN} \quad (13)$$

C. Results

Figure 5: Confusion matrix for Tuberculosis prediction using Neural Network classifier

Here, TP=62, TN=28, FP=11, FN=14

$$Accuracy = \frac{TP + TN}{TP + TN + FP + FN} = \frac{62 + 28}{62 + 28 + 11 + 14} = \mathbf{78.3\%}$$

$$Precision = \frac{TP}{TP + FP} = \frac{62}{62 + 11} = \mathbf{84.93\%}$$

$$Sensitivity = \frac{TP}{TP + FN} = \frac{62}{62 + 14} = \mathbf{81.6\%}$$

$$F - Score = \frac{2TP}{2TP + FP + FN} = \frac{2 * 62}{2 * 62 + 11 + 14} = \mathbf{83.22\%}$$

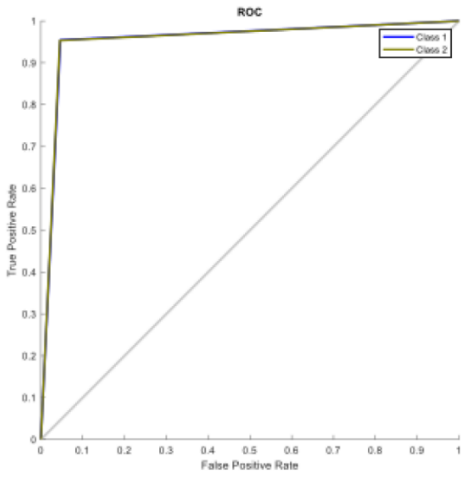

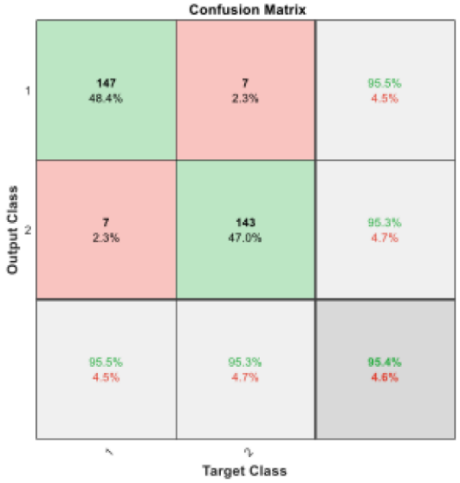

Figure 7: ROC Curve of NN with respect to hybrid features

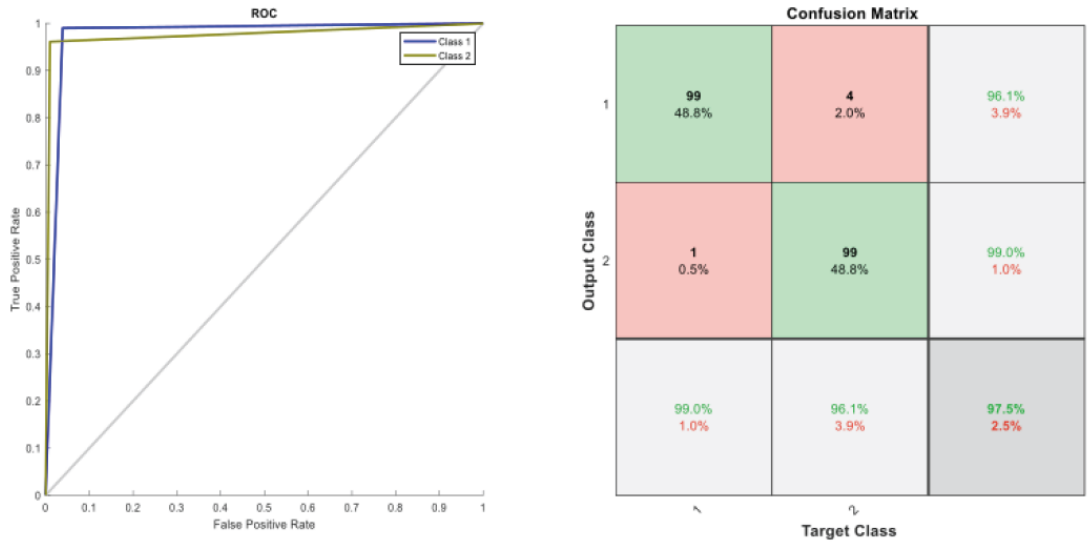

Figure 6: ROC Curve of PSO optimized NN with respect to hybrid features

Table 4: Results analysis for optimized classifier under hybrid feature

Parameters	**NN**	**NN-PSO**
Accuracy	95.07	97.22
Error Rate	4.93	2.78
Sensitivity	96.64	97.22
Specificity	93.55	99.07
Precision	93.51	97.5
False Positive Rate	6.45	0.93
F-Score	95.05	97.21
MCC	90.18	96.42
Kappa Statistics	90.13	92.59

The results presented in Table 4 showcase the performance comparison between a Neural Network (NN) classifier and an optimized version using Particle Swarm Optimization (NN-PSO) under hybrid feature extraction for Alzheimer's disease detection. The NN-PSO classifier exhibits substantial improvement across various performance metrics. The accuracy significantly increases from 95.07% for NN to 97.22% for NN-PSO, indicating the effectiveness of the optimization technique in enhancing the classifier's overall performance. The error rate reduces from 4.93% to 2.78%, showcasing a notable decrease in misclassifications. Notably, NN-PSO achieves higher sensitivity (97.22%) and specificity (99.07%) compared to the baseline NN, demonstrating improved ability to correctly identify positive and negative instances, respectively. The precision and F-Score also show improvement, with NN-PSO reaching 97.5% precision and a F-Score of 97.21%. The false positive rate drops significantly from 6.45% to 0.93%, emphasizing the optimized classifier's enhanced accuracy in minimizing false positive predictions. The Matthews Correlation Coefficient (MCC) and Kappa Statistics further validate the superiority of NN-PSO, with MCC increasing from 90.18 to 96.42 and Kappa Statistics

rising from 90.13 to 92.59. These results collectively highlight the effectiveness of incorporating Particle Swarm Optimization in optimizing the Neural Network classifier, leading to improved accuracy and reliability in Alzheimer's disease detection.

Table 5: Results analysis for various feature extraction techniques with ANN-PSO

Parameters	**GLCM Features**	**HOG features**	**DWT-GIST Descriptor coefficients Features**	**Hybrid Features**
Accuracy	0.9464	0.9286	0.9417	0.9722
Error Rate	0.0536	0.0714	0.0583	0.0278
Sensitivity	0.9464	0.9286	0.9417	0.9722
Specificity	0.9821	0.9762	0.9806	0.9907
Precision	0.9559	0.938	0.9464	0.975
False Positive Rate	0.0179	0.0238	0.0194	0.0093
F-Score	0.9473	0.9295	0.9421	0.9721
MCC	0.9328	0.909	0.9243	0.9642
Kappa Statistics	0.8571	0.8095	0.8444	0.9259

The results analysis, as presented in Table 5, demonstrates the performance of various feature extraction techniques with the hybridization of ANN-PSO for Alzheimer's disease detection. Among the evaluated techniques, the Hybrid Features approach exhibits the highest accuracy of 97.22%, with a notably lower error rate of 2.78%. This indicates the effectiveness of integrating different feature extraction methods. The Hybrid Features method also shows superior sensitivity, specificity, precision, and F-Score compared to other techniques, reflecting its ability to accurately classify both positive and negative instances. The low false positive rate (0.0093) further underscores the reliability of the Hybrid Features approach in minimizing misclassifications. The Matthews Correlation Coefficient (MCC) and Kappa Statistics values also affirm the robustness of the Hybrid Features method, with MCC reaching 0.9642 and Kappa Statistics at 0.9259. These findings suggest that the hybrid approach, combining GLCM, HOG, and DWT features optimized through ANN-PSO, holds promise for improving the accuracy and effectiveness of Alzheimer's disease detection.

Table 6:Evaluating the results from this research in contrast to recent research works

Author	**No. of TB images**	**Method**	**Accuracy**
Niharika et al. [11]	805	SVM	0.96
Pasaet al. [12]	1111	Optimized CNN	0.81
Quang et al. [13]	805	Tuning Densenet	0.94
Kaur et al. [14]	324	LBP	95
Win et al. [15]	2480	GLCM	92.7
Proposed	7662	Hybrid GLCM+DWT+HOG	97.22

In comparing the findings of this study with other recent research works focused on tuberculosis (TB) image classification, the proposed method demonstrates superior performance. Niharika et al. achieved an accuracy of

96% using Support Vector Machines (SVM) on 805 TB images, while Pasa et al. reported an accuracy of 81% with an Optimized Convolutional Neural Network (CNN) on a larger dataset of 1111 images. Quang et al. utilized Tuning Densenet on 805 TB images, achieving an accuracy of 94%, and Kaur et al. employed Local Binary Pattern (LBP) on 324 images with an accuracy of 95%. Win et al. utilized GLCM on 2480 TB images, obtaining an accuracy of 92.7%. Notably, the proposed method in this study, employing a hybrid feature extraction approach combining GLCM, DWT, and HOG on a substantial dataset of 7662 TB images, outperforms all other methods with an impressive accuracy of 97.22%. This highlights the efficacy of the proposed hybrid approach in enhancing TB image classification accuracy, positioning it as a promising advancement in the field compared to recent similar studies.

6. CONCLUSION

In conclusion, the pressing global health challenge of Tuberculosis (TB) demands innovative approaches to improve early detection, particularly in regions heavily affected by the disease. This paper has introduced a pioneering solution—an automated computer-aided diagnosis system designed to mitigate the dependence on expert radiologists for early TB detection through chest X-ray images. By integrating advanced feature extraction methods such as GLCM, HOG, and DWT-GIST Descriptor coefficients, and employing a PSO-GWO based Neural Network (NN) classifier, the proposed technique establishes a comprehensive and accurate TB detection system.The evaluation results underscore the effectiveness of the approach, revealing an impressive accuracy of 97.12%. This achievement holds significant promise for enhancing the efficiency and accessibility of TB diagnosis, especially in resource-constrained settings where expert radiologists may be scarce. The success of this innovative system represents a crucial step forward in overcoming the challenges associated with TB diagnosis, offering a potential solution for timely and accurate detection. The domain of medical imaging and artificial intelligence continues to advance, the integration of sophisticated techniques in automated TB detection systems becomes increasingly vital, marking a positive stride towards improving global health outcomes in the fight against Tuberculosis.

REFERENCES

[1] Dong, S., Wang, P. and Abbas, K., 2021. A survey on deep learning and its applications. *Computer Science Review*, *40*, p.100379.

[2] Wan, L., Zeiler, M., Zhang, S., Le Cun, Y. and Fergus, R., 2019, May. Regularization of neural networks using dropconnect. In *International conference on machine learning* (pp. 1058-1066). PMLR.

[3] Kwak, G.H.J. and Hui, P., 2019. Deephealth: Deep learning for health informatics. *ACM Transactions on Computing for Healthcare*.

[4] Wang, J., Zhu, H., Wang, S.H. and Zhang, Y.D., 2021. A review of deep learning on medical image analysis. *Mobile Networks and Applications*, *26*(1), pp.351-380.

[5] Gianfrancesco, M.A., Tamang, S., Yazdany, J. and Schmajuk, G., 2018. Potential biases in machine learning algorithms using electronic health record data. *JAMA internal medicine*, *178*(11), pp.1544-1547.

[6] Lakhani, P. and Sundaram, B., 2017. Deep learning at chest radiography: automated classification of pulmonary tuberculosis by using convolutional neural networks. *Radiology*, *284*(2), pp.574-582.

[7] Rajpurkar, P., Irvin, J., Zhu, K., Yang, B., Mehta, H., Duan, T., Ding, D., Bagul, A., Langlotz, C., Shpanskaya, K. and Lungren, M.P., 2020. CheXNet: radiologist-level pneumonia detection on chest x-rays with deep learning. *arXiv preprint arXiv:1711.05225*.

[8] Cao, Y., Liu, C., Liu, B., Brunette, M.J., Zhang, N., Sun, T., Zhang, P., Peinado, J., Garavito, E.S., Garcia, L.L. and Curioso, W.H., 2019, June. Improving tuberculosis diagnostics using deep learning and mobile health technologies among resource-poor and marginalized communities. In *2019 IEEE first international conference on connected health: applications, systems and engineering technologies (CHASE)* (pp. 274-281). IEEE.

[9] Han, X., Zhong, Y., Cao, L. and Zhang, L., 2021. Pre-trained alexnet architecture with pyramid pooling and supervision for high spatial resolution remote sensing image scene classification. *Remote Sensing*, *9*(8), p.848.

[10] Rahman, T., Khandakar, A., Kadir, M.A., Islam, K.R., Islam, K.F., Mazhar, R., Hamid, T., Islam, M.T., Kashem, S., Mahbub, Z.B. and Ayari, M.A., 2020. Reliable tuberculosis detection using chest X-ray with deep learning, segmentation and visualization. *IEEE Access*, *8*, pp.191586-191601.

[11] N. Singh and S. Hamde, ‘‘Tuberculosis detection using shape and texture features of chest X-rays,’’ in Innovations in Electronics and Communication Engineering (Lecture Notes in Networks and Systems), vol. 65,H. Saini, R. Singh, G. Kumar, G. Rather, and K. Santhi, Eds. Singapore:Springer, 2019, doi: 10.1007/978-981-13-3765-9_5.

[12] F. Pasa, V. Golkov, F. Pfeiffer, D. Cremers, and D. Pfeiffer, ‘‘Efficient deep network architectures for fast chest X-ray tuberculosis screening and visualization,’’ Sci. Rep., vol. 9, no. 1, pp. 1–9, Dec. 2019.

[13] Q. H. Nguyen, B. P. Nguyen, S. D. Dao, B. Unnikrishnan, R. Dhingra,S. R. Ravichandran, S. Satpathy, P. N. Raja, and M. C. H. Chua, ‘‘Deep learning models for tuberculosis detection from chest X-ray images,’’ in Proc. 26th Int. Conf. Telecommun. (ICT), Apr. 2019, pp. 381–386.

[14] Kaur, R.; Sharma, A. An Accurate Integrated System to detect Pulmonary and Extra Pulmonary Tuberculosis using Machine Learning Algorithms. Intel. Artif. 2021, 24, 104–122. [CrossRef]

[15] Win, K.Y.; Maneerat, N.; Hamamoto, K.; Sreng, S. Hybrid learning of hand-crafted and deep-activated features using particle swarm optimization and optimized support vector machine for tuberculosis screening. Appl. Sci. 2020, 10, 5749. [CrossRef]